

Manuscript version: Author's Accepted Manuscript

The version presented in WRAP is the author's accepted manuscript and may differ from the published version or Version of Record.

Persistent WRAP URL:

<http://wrap.warwick.ac.uk/160558>

How to cite:

Please refer to published version for the most recent bibliographic citation information.

Copyright and reuse:

The Warwick Research Archive Portal (WRAP) makes this work by researchers of the University of Warwick available open access under the following conditions.

Copyright © and all moral rights to the version of the paper presented here belong to the individual author(s) and/or other copyright owners. To the extent reasonable and practicable the material made available in WRAP has been checked for eligibility before being made available.

Copies of full items can be used for personal research or study, educational, or not-for-profit purposes without prior permission or charge. Provided that the authors, title and full bibliographic details are credited, a hyperlink and/or URL is given for the original metadata page and the content is not changed in any way.

Publisher's statement:

Please refer to the repository item page, publisher's statement section, for further information.

For more information, please contact the WRAP Team at: wrap@warwick.ac.uk.

Ray Tracing 3D Source Modelling for Optical Reflectance Sensing with Wireless Ranging Application

1st Vlad Marsic
University of Warwick
WMG
Coventry, UK
v.marsic@warwick.ac.uk

2nd Erik Kampert
University of Warwick
WMG
Coventry, UK
e.kampert@warwick.ac.uk

3rd Matthew D. Higgins
University of Warwick
WMG
Coventry, UK
m.higgins@warwick.ac.uk

Abstract— This study delivers a powerful comparison case for six of the most common ray tracing (RT) source models. It demonstrates that in the early stages of the RT algorithm, when only the ray-geometry intersection and ray-reflectance are introduced, the ray source modelling is a pivotal event in the simulation. The six models are compared in a large three-dimensional (3D) scenario of the well-known double-slit experiment, with the comparison metrics delivered by the number of rays that intersect the back screen and the total simulation time. The numerical results for a variable number of 2,000; 10,000; 25,000 and 100,000 rays that emulate each of the six source models, are accompanied by the simulation's visual output samples to eliminate abstract ambiguities. This work's main contribution applies directly to the RT simulation for wireless ranging, since scientific programming environments such as MATLAB are extensively utilised in this research field, which provide the required modelling customisation. Moreover, for machine sensing areas involving optical ranging or light detection and ranging (LIDAR) mapping, the presented study provides valuable information about efficient modelling for ray fascicle launching. Furthermore, since RT simulations enable the latest performances in the gaming and animation industries, the basic and clear information presented in this work supports the next generation of their developers in the delivery of hardware and software implementations.

Keywords—ray tracing, shooting, casting, source, modelling

I. INTRODUCTION

Recent technological advancements paved the way for accessible laser-based sensors and powerful computational simulation environments. Ray tracing (RT) simulation is one of the most representative geometrical optics (GO) techniques. Apart from its main utilisation in graphical computing and realistic image rendering [1, 2], the technique is substantially employed for scientific simulations of large scenarios and complex scenery such as used in astrophysics [3, 4], radio propagation [5, 6], thermal and fluid dynamics [7, 8].

Despite its popularity, its intensive utilisation and the constant advancements in its acceleration techniques, RT source modelling for basic reflectance implementation is an often-overlooked research area. A user frequently starts from the hypothesis that the software package delivering the RT uses the best option for the ray source simulation, or the default ray casting implementation delivers a more accurate result if increasing the initial number of rays: the solution resolution relates directly to the scenario's ray sampling density. The concept of high spatial resolution delivering a more accurate set of results is adopted from full wave electromagnetics (EM) modelling. The acknowledged method

of finite difference time domain (FDTD) [9] illustrates a strong example for the full wave geometry resolution adaptation concept, through recommending its smallest geometry element to be at least ten times smaller than the simulated signal wavelength [10]. Increasing the ray casting number may in some cases improve the probability of hitting the designated area, however, examples of rays propagating parallel to the ground plane and the target walls or diverging in the target's vicinity, such as for plane or spherical wave approximations, may result in insignificant or no improvement.

Despite the RT method's rich history and its field applications providing a plethora of comprehensive source modelling guidance focusing on complexity and efficiency [11], to the best of the authors' literature review and knowledge, a comparison between various ray casting or shooting techniques applied to a known three-dimensional (3D) scenario, and measured by quantitative metrics such as target successful hit or miss and their associated computational times, does not exist. Moreover, a visual output sample of such an experiment is highly beneficial for understanding the simulation steps in the new emerging areas of robot wireless sensing and smart vehicle light detection and ranging (LIDAR) mapping technologies.

This study demonstrates the importance of RT source modelling for reflectance implementation by employing six different methods and applying them to a large-scale 3D double-slit experiment [12] simulation for case illustration. The number of rays emulating a point transmitter (TX) is varied to exemplify that some models may improve their receiving rate by increasing the ray density, whereas others maintain a constant rate. The flat plane behind the two narrow slits has the functionality of a receiver (RX), the point distribution resulting from straight line segments of rays intersected with the scenario's geometry planes, providing a graphical illustration of each TX type's potential.

The overall goal of this study is to deliver powerful 3D RT source modelling examples, which can invalidate persistent simulation misconceptions, and encourage the research benefiting from access to a scientific programming environment such as MATLAB to use in solving wireless communications problems, rather than selecting dedicated software packages that offer default solutions and "black-box" implementations.

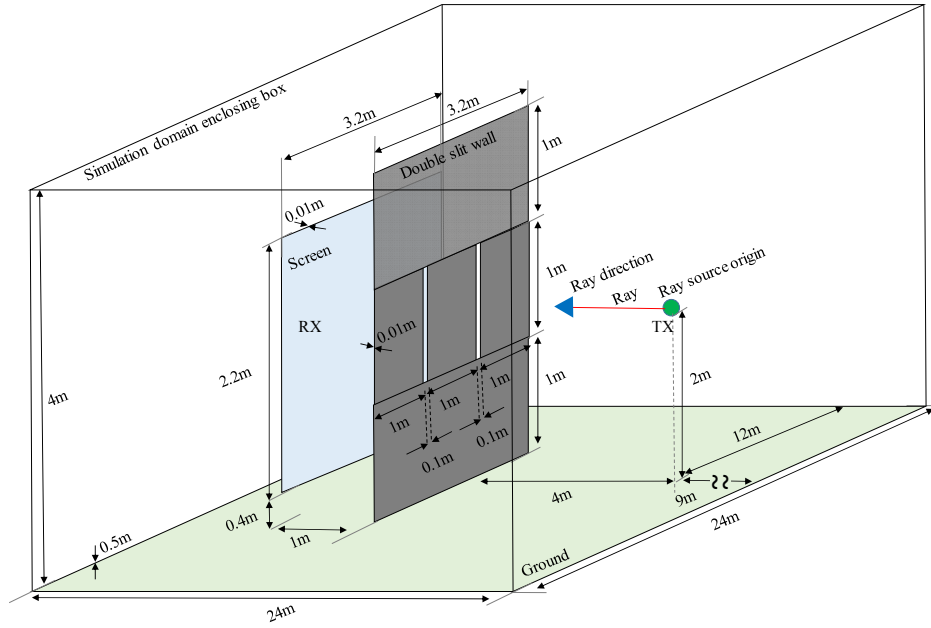


Figure 1. RT simulation environment. The ray origin is equivalent with a point transmitter TX, whereas the screen is associated with a receiver RX. The geometric dimensions and labels are provided, but for increased clarity the schematic is not made to scale.

II. METHODOLOGY

The RT source origin is placed inside a virtual 3D test environment represented by a large rectangular box with dimensions $24 \times 24 \times 4$ m. The reflective plane accommodating the two narrow slits and the one behind it representing the receiving screen, are positioned parallel to each other and both perpendicular to the ground surface. Whereas the slit wall rests its base on the ground, the back screen is 0.4 m raised above the floor and centred relative to the front wall. This illustrates a scenario where multiple reflected rays may escape due to consecutive reflections under the screen and not contribute to the overall reception. The quantitative reception principle is based on the ray's emulation as a straight-line segment and its possible intersection with a geometrical shape in the simulation environment: a successful intersection is considered a hit and marked as a dot or X on the surface of incidence, while a miss

is left unmarked. The total number of dots or hits on a predefined receiver geometry, such as the back screen in this study, represents the quantitative signal reception, and the percentage of hits with respect to the initial ray shot number provides a scale of comparison between different ray source models sharing the same origin. It is straightforward to notice that some methods that optimise the ray cast towards a predefined target will take a toll on the total simulation time, numerous algorithms move this action from the processing or on-line phase to a separate pre-processing or off-line stage. The work presented here accounts for all the ray source simulation times in the on-line phase, to provide a second measure for the comparison of the six different models. Since the complete scenario's geometry contains only rectangular shapes, delivering a total triangular mesh of 72 faces, no acceleration methods through hardware [13] or software [14, 15] have been employed. The RT programming for this work has been implemented on MATLAB R2019b running on a

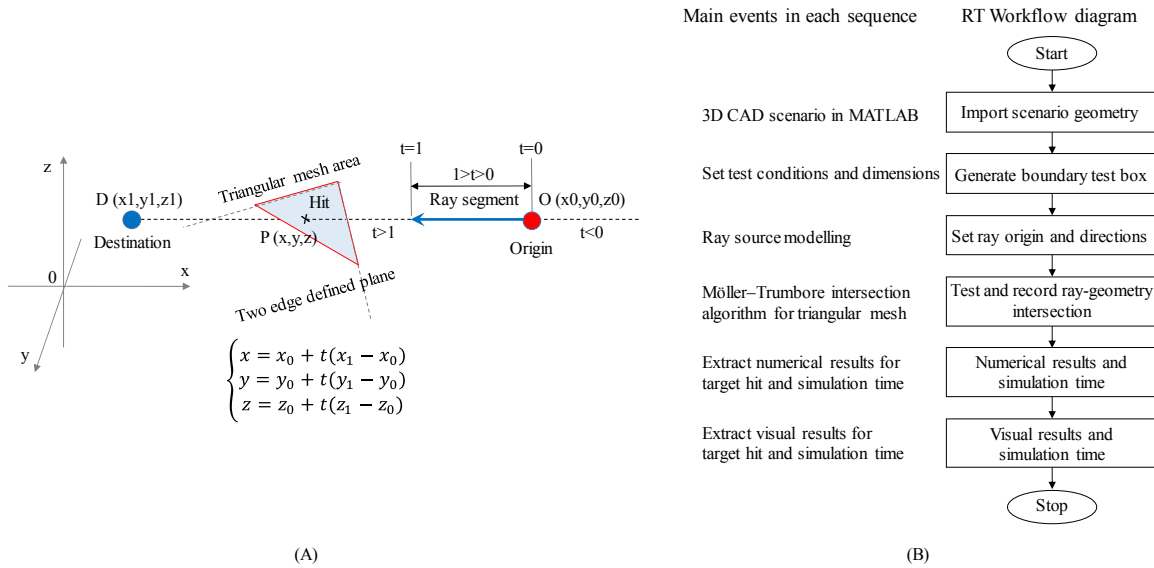


Figure 2. (A) Representation of the 3D RT simulation parametric ray-triangle intersection (B) Algorithm used to generate the comparison data for the six different ray source models.

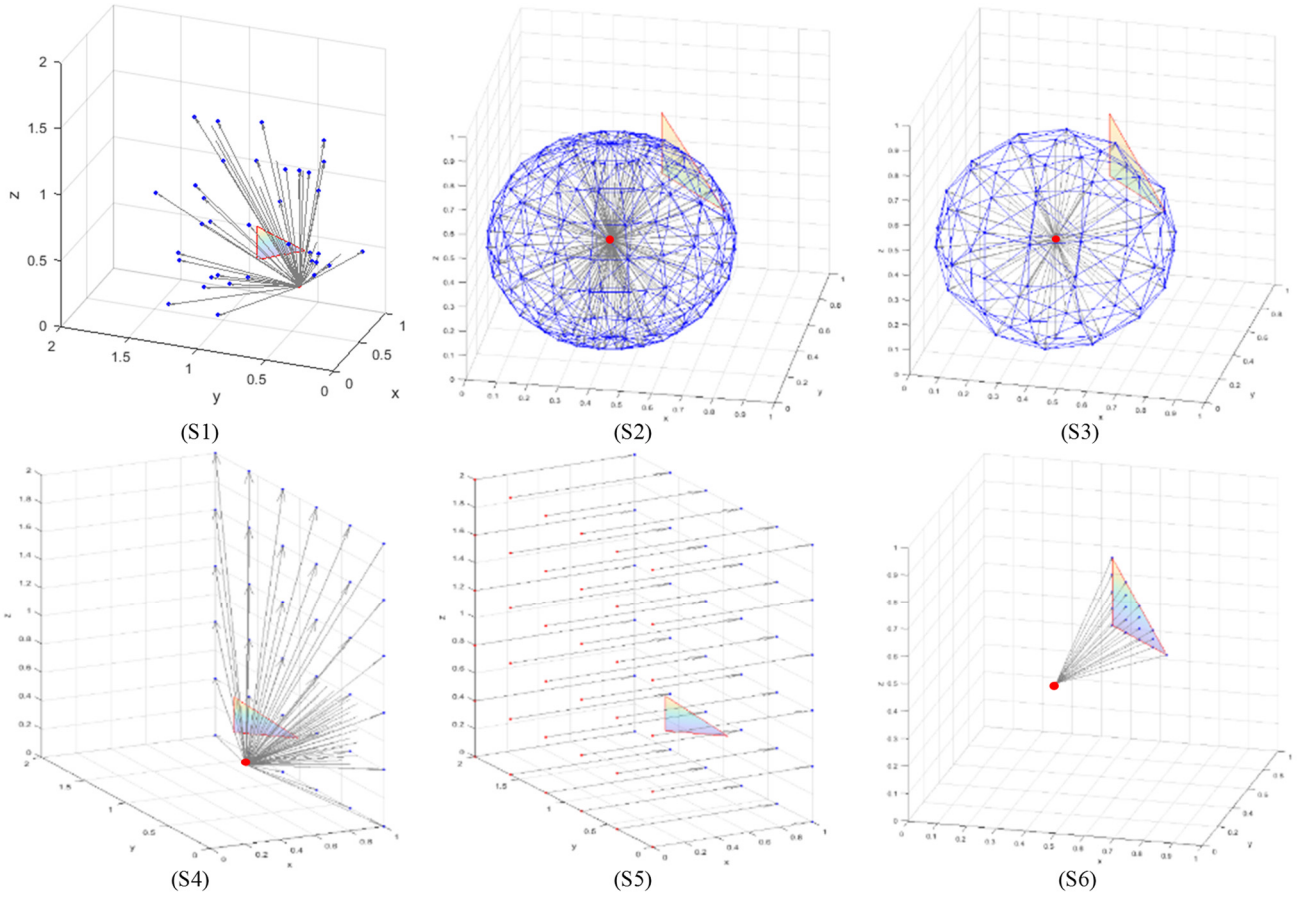


Figure 3. 3D ray source model's direction points generated by a (S1) 3D random function; (S2) sphere resulting from azimuth and elevation angle; (S3) sphere resulting from octahedral edge split; (S4) enclosure box set on an orthogonal grid – one wall; (S5) enclosure box set on an orthogonal grid – two opposite walls; (S6) digitised target triangle – backwards super-sampling. The ray source origin is illustrated as a red dot, the rays as grey arrows and the direction points as blue dots.

Windows 10 system powered by an Intel Xeon E5-1620 v2 3.7 GHz four core central processing unit (CPU). Fig. 1 presents the 3D virtual test environment with the relative positions and sizes of the various shapes composing the scenario. Whereas the shapes' main aim is to transform the double-slit experiment in a large-scale structure, including fine details down to 0.01 m, the origin of the ray source can be associated with a ranging system installed on top of a vehicle or manufacturing robot. The simplified 3D parametrical representation for a straight-line ray emulation and a 2D plane is presented in Fig. 2 A, [16]. The relation between the ray's origin O , the direction D , and a two-edge defined triangular plane as described by the Möller–Trumbore intersection algorithm [17], is illustrated in Fig. 2 B, enriching the software implementation details presented as a workflow diagram. The scenario geometry has been designed in FreeCAD and imported in MATLAB in the stereolithographic (STL) format. The ground plane has been included to provide simulation realism, whereas the enclosing scenario box walls are considered perfect ray absorbers.

By considering the general case of omnidirectional propagation, the destination points can be generated in various ways, such as those presented in Fig. 3 for the six distinct ray source models selected for this work:

Source one (S1) is modelled with all its ray destinations being 3D random point coordinates associated with the Cartesian grid of the scenario's six enclosing box walls. The source origin is unique and fixed in a predefined position, in front of the reflective plane containing the two slits. The random point distribution is a common technique employed by spatial sampling methods [18] to deliver an unbiased overall homogeneity.

Source two (S2) is generated as its complete set of ray destination points are producing a spherical surface with its centre on the source's origin. Spherical wave propagation simulation is based on the principle that all surface points are equidistantly distributed. In practice, the principle raises great modelling challenges as the discrete points on a spherical

Table 1. 3D double-slit experiment ray screen-hit percentage for six different ray source (S) models and various ray densities of 2,000; 10,000; 25,000 and 100,000 rays.

Ray No	S1	S2	S3	S4	S5	S6
100,000	1.62	0.19	0.32	0.96	0.30	9.00
25,000	1.58	0.21	0.33	0.79	0.22	9.38
10,000	1.49	0.00	0.58	0.72	0.23	10.54
2,000	1.81	0.00	0.13	0.60	0.20	10.46

Table 2. 3D double-slit experiment running simulation times in seconds without graphics for six different ray source (S) models and ray densities of 2,000; 10,000; 25,000 and 100,000 rays.

Ray No	S1	S2	S3	S4	S5	S6
100,000	7.01	8.58	8.53	10.41	4.98	15.62
25,000	1.90	1.90	1.99	2.08	1.52	2.98
10,000	1.24	1.17	1.15	1.44	1.19	1.58
2,000	1.11	0.98	0.95	1.07	0.99	1.18

surface may be constructed separately by approximate equal angles or sharing roughly equal edges. To generate an angle-based distribution, the azimuth and elevation angles are generated from the origin and then transformed from spherical coordinates to Cartesian points. By producing the same number of points for all the sphere's elevation planes, the method shows a higher point density to the sphere's top and bottom, hence equidistant angles produce a nonhomogeneous point distribution. S2 follows this generation method. Such type of source model is characteristic for scanning obtained by a rotating sensor or array, and if a full circle is completed, systematically increasing its elevation angle.

Source three (S3) is based on a different rule for the spherical surface generation. To construct an equal edge based spherical distribution, a method for iterative splitting of the

edges from a regular polyhedron is suggested [19]. In this study case, an octahedral triangular mesh is used. The method produces uniformly distributed points on a spherical surface, with their amount controlled by the number of iterative edge splitting steps. The angles are difficult to collect and interrogate in an orderly manner, and the number of total points, respectively ray directions, is not prone to arbitrary values, since it depends on the iterative splitting process.

Source four (S4) is emulated with the destination points on a virtual uniformly spaced grid attached to the six walls of the enclosing test box. The resulting points are separated by an adaptable resolution step allowing arbitrary values for the total associated ray number. For greater clarity, in Fig. 3 S4 illustrates the method only for one of the six enclosing walls. The spatial homogeneity for the ray direction points is reached at the orthogonal grid level, emulating the grid projection on

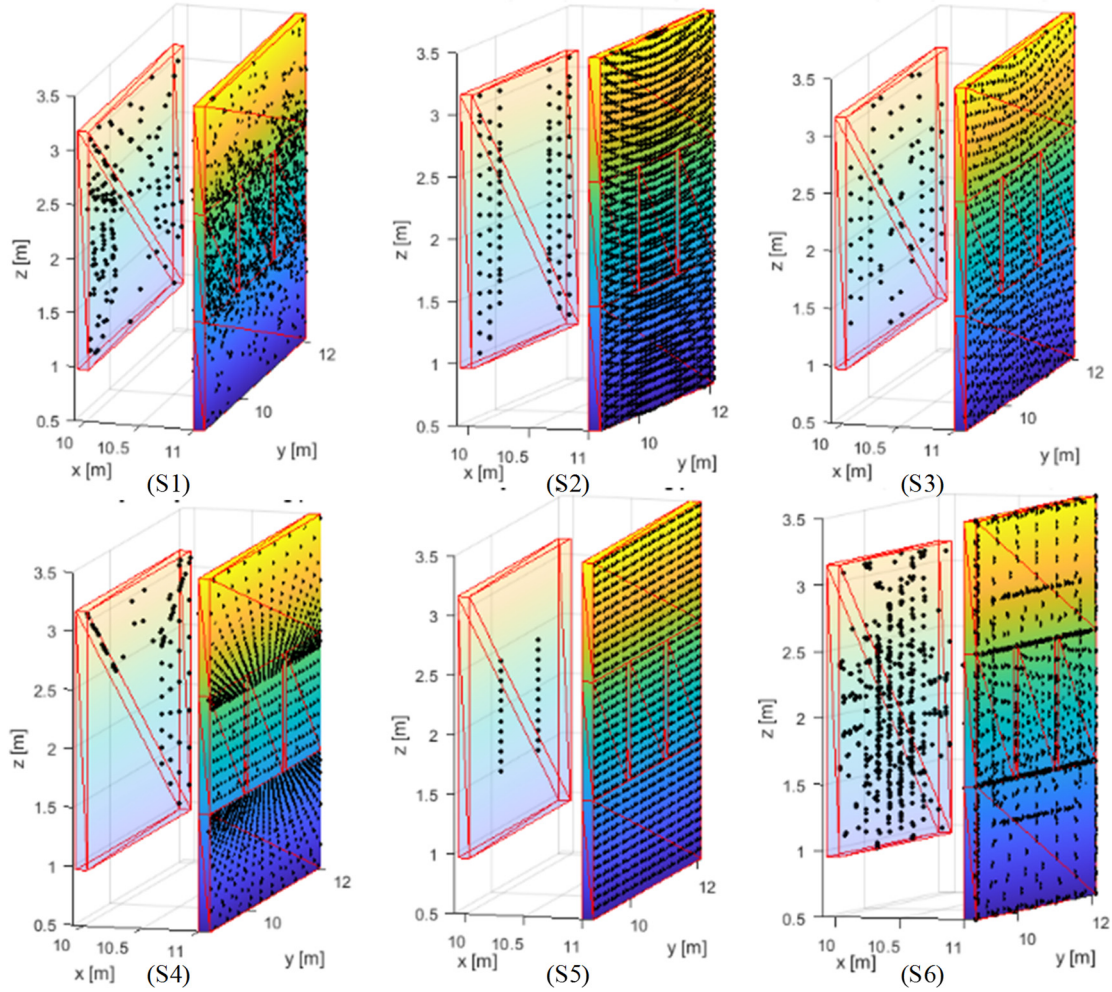


Figure 4. 3D double-slit experiment "target "hit" visualization (black dots) for 25,000 rays using the source model: (S1) 3D random function; (S2) sphere resulting from azimuth and elevation angles; (S3) sphere resulting from octahedral edge split; (S4) enclosure box set on an orthogonal grid – one wall; (S5) enclosure box set on an orthogonal grid – two opposite walls; (S6) digitised target triangle – backwards super-sampling.

a spherical surface. However, to obtain the relative equal distributed point mesh through this method, the common rays' origin needs to be positioned in the middle of a cubic grid, for this example case in the middle of a cubic enclosing test box.

Source five (S5) is modelled with the destination points attached to one face of the test box's virtual grid and pointing backwards from the ray source origin mirrored on the opposite test box wall. This technique produces a ray fascicle parallel to the ground, propagating in planes of equal phase, and is often called plane wave simulation as it is used to model the EM far-field. This method does not generate the rays from the source's common origin, but from a plane perpendicular to the ground and containing the common origin. The direction points' spatial homogeneity is reached at rectangular grid level like for S4, however unlike that obtained in an array point representation of space.

Source six (S6) is constructed by backwards casting, the ray starts from the geometrical target towards the source [20], and the mesh's triangular geometry is super-sampled by generating more than one ray for every geometrical simplex. To generate the beam's direction points from the scenario geometry, each shape requires a digitisation or rasterization that transforms the 2D or 3D meshed geometry in a point cloud. The number of points generated per area or volume unit may be delivered in the RT simulation by following various rules. For this study, each mesh's triangle generates a constant number of points, independent from spatial sizes, as demonstrated in [21]. By implementing this procedure, any minor geometrical feature in the scenario, such as the thin sheet's thickness, is accounted for and is given the same status as a large detail.

III. RESULTS AND DISCUSSION

The first result set displays the percentage of ray intersections with the RX back screen resulting from an initial variable number of rays modelling the TX source. Since the screen is considered during the simulation as a reflective surface, some rays will bounce between the slit wall and the RX plane producing multiple hits, others will intersect only once if their incident angle to the surface's normal is 90° , and the rest will not pass through the two-slit wall and is absorbed by the enclosure box's boundary walls. Table 1 shows the quantitative result as a percentage metric. It can be observed, that despite using the same number of initial shooting rays when increasing the beam density, the methods using S1, S5 and S6 tend to deliver a constant result, whereas S2 and S4 gradually improve their hit rate, and S3 displays a local optimum. The sources S2 and S6 deliver the minimum and maximum successful receptions, respectively, and S2 exhibits a poor directionality due to its parallel stacked circular planes of equal angle, whereas S6 is constructed from the scenario's geometry backwards to the source, and therefore displays a high efficiency. The 3D random direction generation of S1 accounts for the second-best hit performance after S6. And despite this being approximatively nine times lower if compared with each other, S1 still delivers an almost double percentage compared to the remaining four sources. Contrary to expectations, the source S2 misses the two slits' entrances completely for an initial number of up to 10,000 rays, whereas the parallel beams generated by S5, deliver a better performance for all ray densities, although out of focus, perpendicular to the screen's surface, and producing no more than one hit per ray. Comparing S3 and S4, which both follow a homogenous spatial distribution for their direction points, S3

on a spherical uniform grid and S4 on a rectangular orthogonal spacing, S4 delivers an almost double hit count on the RX plane.

From the comparison in Table 2 of the on-line RT simulation durations for the results presented in Table 1, it can be observed that despite S6 producing the best RX hit results, it performs slowest because it requires additional time to digitise the 3D scenario. The random ray direction generation of S1 displays similar low simulation times as for the sources S2, S3 and S4, whereas the fastest execution is delivered by the parallel ray fronts modelling source S5. It should be noted that based on these results for small experimental scenarios, such as used in this study, with a total number of faces smaller than 1,000 and only up to ten reflections, the implementation of RT accelerating methods may not be necessary.

To visually assess the picture sketched by the numerical results recorded in Table 1 and 2, the simulation's receiving screen and the two-slit wall are shown in Fig. 4, illustrating a 25,000-ray source modelling example. It can be observed that each source's specific distribution rule may be accounted for by the back screen's pattern of dots. For S1 it displays a random arrangement; for S2 and S3 it delivers a fringed pattern with a higher density on the left and right sides, accordingly to progressive spatial dispersion of their spherical radii; S4 shows point fringes on the upper screen's triangular mesh as the grid associated with the enclosing box is rectangular and not cubic, and the source origin is not central to the scenario; S5 produces two projection bands of the slits' openings on the screen as a result of its perpendicular incidence on the double-slit wall's geometry; and S6 delivers a fringe distribution similar to a diffraction pattern, however this is due to the multiple reflections generated by the slit openings wall thickness.

IV. POTENTIAL REAL-WORLD IMPLEMENTATIONS OF THE MODELLED RAY SOURCES

Besides the obvious direct benefit of the RT source modelling for the 3D simulation environment, possible relationships with practical sensing and measurement applications exist for the six discussed methods. Fig. 5 succinctly illustrates six real-world systems, each corresponding to a potential application of one of the distinct source models introduced in this work:

S1 may be used for target characterisation if particles or an object randomly scatter a beam of light [22] or an electron fascicle [23] and the result is recorded on a detector screen.

The azimuth and elevation ray direction sphere used for modelling S2 may be used for a LIDAR system [24] casting a laser fascicle or a beam array to an unknown environment while spinning around its vertical axis.

A spherical sensor array as used in acoustics [25] with its equidistant sensor positioning on a spherical surface may behave as S3. However, as the probe can be passively sampling the surrounding acoustic field, the RT backwards ray casting technique is imposed.

A phased antenna array for a radar system with beam steering towards a certain target [26] may be emulated by the grid ray model with backwards ray casting towards the origin, as introduced by S4.

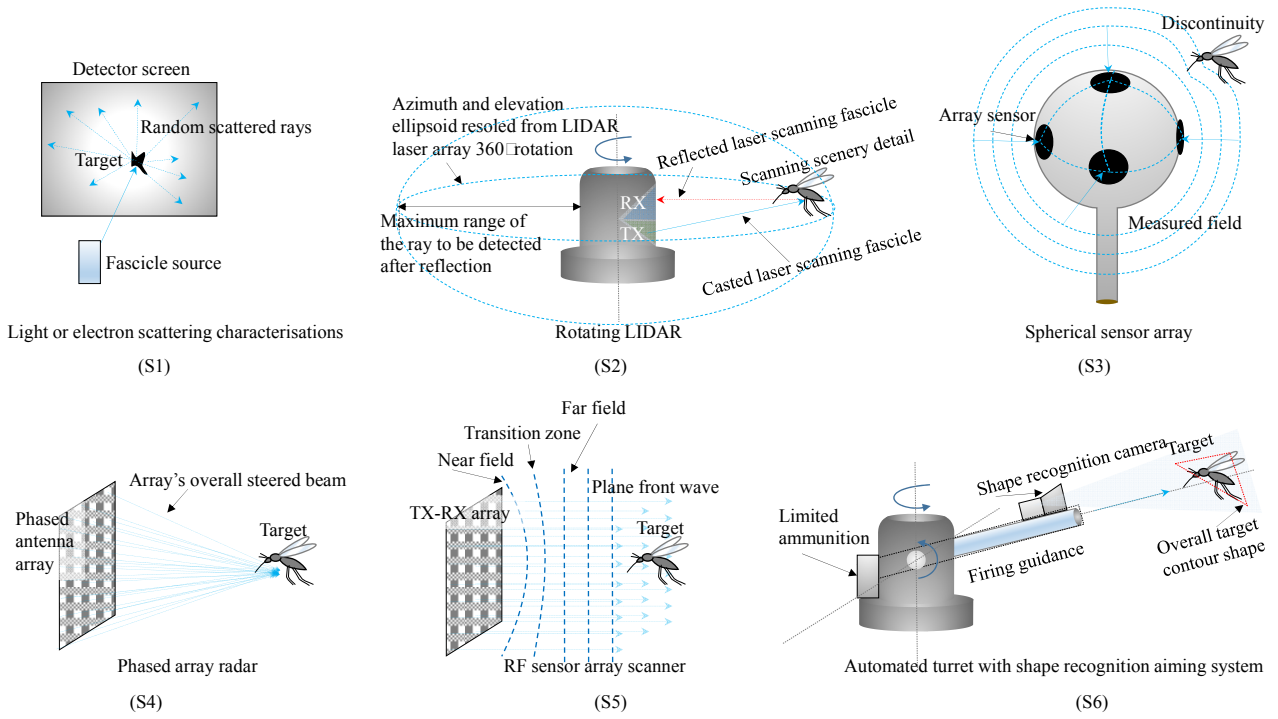


Figure 5. A selection of real-world sensing system examples with their potential relation to the ray source models presented in this study. Random scattering of light or an electron fascicle (S1); 360° spinning LIDAR (S2); 3D spherical acoustic field probe (S3); planar uniform phased antenna array radar (S4); planar uniform distributed scanning RF sensor array (S5); automatic shooting spinning turret with target contour recognition system (S6).

Whereas in the far field from the transmitter, a plane-wave is generally considered as a wavefront propagating parallel to the ground, a better visual illustration may be provided by S5 for an RF millimetre wave sensor array composed of independent TX/RX units, for example in a security scanner [27].

The source modelling presented for S6 relies on a pre-processing stage in which the scenario geometry's faces are identified and points are generated as ray directions through super-sampling. The highly efficient S6 and its association with the target's points, has clear similarities with a turret that uses a target's contours from an additional video system, to decide how to use its limited reserves [28].

An additional application for quantitative RT simulation, not often illustrated in literature, is the synthesis of a sensing system based on a specific behaviour and geometrical structure. For example, if a ray source casts its rays to a rectangular box with one wall missing, then if the ray source is perpendicular to the box's walls, a receiving surface placed inside the box will record a ray miss, and if the ray source is

perpendicular to the missing wall, then the receiver inside will record a ray hit. This binary behaviour of the receiver for different positions of the ray source can be translated into a real-world scenario through the design of a directional RF sensor placed inside an enclosure that is only open at a single side. The binary behaviour will then manifest itself by attenuation of the signal through the enclosure's walls and providing a good detection for a line-of-sight (LOS) signal. As an example in Fig. 6 A, the simulated positional response to the ray source from a receiver inside a rectangular reflective box with one missing wall has been created and tested in the real-world by completely encasing an RF sensor based on the IEEE 802.15.4 standard inside a cylindrical metal enclosure with one opening [29]. Fig. 6 B illustrates the 3D schematic of the resulting real-world sensor based on the MRF24J40MA 2.4 GHz transceiver, with its omnidirectional radiation pattern without the metal enclosure illustrated in Fig. 6 C, and the directionality of the encased sensor presented in Fig. 6 D.

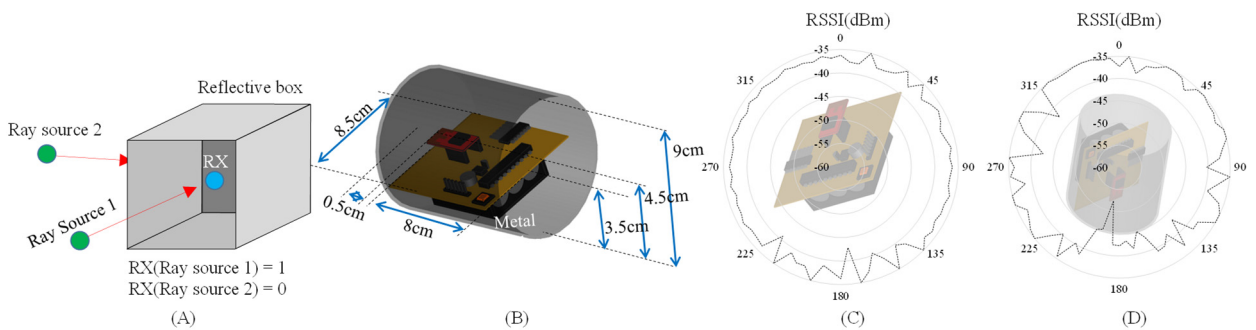


Figure 6. A) The quantitative RT RF sensor reproducing the ray source's position dependance of a receiver RX placed inside a reflective open box; B) the synthesized RF sensor based on the MRF24J40MA 2.4 GHz transceiver inside a cylindrical metal enclosure; C) omnidirectional radiation pattern of the RF sensor without an enclosure; D) directional radiation pattern of the enclosed RF sensor.

V. CONCLUSION AND FURTHER WORK

This study has demonstrated the importance of RT source modelling for reflectance implementation, showing that different ray casting methods deliver different results despite sharing the same ray density and position towards a 3D target. Moreover, six different ray source models have been illustrated for a large-scale 3D double-slit simulation demonstrating the fitness of RT for substantial scenarios. Comparison metrics have been expressed via their quantitative reception, running times and graphical spatial distribution of successful target ray intersects criteria. Real-world examples of sensor systems that emulate the six ray source models have been presented and a possible RF sensor synthesis from the RT quantitative simulation was discussed as an additional potential application.

The presented results suggest that RT modelling in a generic scientific computing environment, such as MATLAB, may deliver benefits beyond simulation on dedicated platforms. Therefore, the use of traditional coding without modern acceleration methods to solve a variety of RT problems is highly recommended.

ACKNOWLEDGMENT

The authors would like to thank Tom Mizutani, Dr Joshi Harita, David Oxtoby, Dr Alex Mouzakitis, Gunwant Dhadyalla and Professor Paul Jennings for their helpful support. This work was supported through the RACeD Doctorate Programme.

REFERENCES

- [1] M. Slater, A. Steed and Y. Chrysanthou, *Computer graphics and virtual environments: from realism to real-time*, Pearson Education, 2002.
- [2] E. Haines and T. Akenine-Möller, *Ray Tracing Gems: High-Quality and Real-Time Rendering with DXR and Other APIs*, Apress, 2019.
- [3] J. Steinacker, A. Bacmann and T. Henning, "Ray tracing for complex astrophysical high-opacity structures," *The Astrophysical Journal*, vol. 645, no. 2, p. 920, 2006.
- [4] R. Makiya, I. Kayo and E. Komatsu, "Ray-tracing log-normal simulation for weak gravitational lensing: application to the cross-correlation with galaxies," *Journal of Cosmology and Astroparticle Physics*, vol. 3, p. 095, 2021.
- [5] T. Imai, "A survey of efficient ray-tracing techniques for mobile radio propagation analysis," *IEICE Transactions on Communications*, 2016.
- [6] T. Geok, F. Hossain, M. Kamaruddin, N. Rahman, S. Thiagarajah, A. Chiat and C. Liew, "A comprehensive review of efficient ray-tracing techniques for wireless communication," *International Journal on Communications Antenna and Propagation*, vol. 8, no. 2, pp. 123-136, 2018.
- [7] B. Semlitsch, *Advanced ray tracing techniques for simulation of thermal radiation in fluids*, Wien: Technischen Universität Wien, 2010.
- [8] D. Zheng, J. Mei and M. Wang, "Improvement of gas ultrasonic flowmeter measurement non-linearity based on ray tracing method," *IET Science, Measurement & Technology*, vol. 10, no. 6, pp. 602-606, 2016.
- [9] K. S. Kunz and R. J. Luebbers, *The finite difference time domain method for electromagnetics*, CRC press, 1993.
- [10] M. N. O. Sadiku, *Numerical techniques in electromagnetics*, Boca Raton: CRC Press LLC, 2001.
- [11] Szirmay-Kalos and L. a. Márton, "Worst-case versus average case complexity of ray-shooting," *Computing*, vol. 61, no. 2, pp. 103-131, 1998.
- [12] Y. Li, X.-L. Wang, H. Zhao, L.-J. Kong, K. Lou, B. Gu, C. Tu and H.-T. Wang, "Young's two-slit interference of vector light fields," *Optics letters*, vol. 37, no. 11, pp. 1790-1792, 2012.
- [13] J. Peddie, "Ray-Tracing Hardware," in *Ray Tracing: A Tool for All*, Springer Cham, 2019, pp. 129-180.
- [14] A. S. Glassner, "Space subdivision for fast ray tracing," *IEEE Computer Graphics and applications*, vol. 4, no. 10, pp. 15-24, 1984.
- [15] Y. Deng, Y. Ni, Z. Li, S. Mu and W. Zhang, "Toward real-time ray tracing: A survey on hardware acceleration and microarchitecture techniques," *ACM Computing Surveys (CSUR)*, vol. 50, no. 4, pp. 1-41, 2017.
- [16] S. Marschner and P. Shirley, "3.5.2 Line Drawing Using Parametric Line Equations," in *Fundamentals of computer graphics*, CRC Press, 2018, p. 61.
- [17] T. Möller and B. Trumbore, "Fast, minimum storage ray/triangle intersection," *ACM SIGGRAPH*, vol. Courses, no. ACM, p. 7, 2005.
- [18] E. Delmelle, "Spatial Sampling," in *The SAGE handbook of spatial analysis*, 2009, pp. 165-186.
- [19] G. Durgin, N. Patwari and T. S. Rappaport, "An advanced 3D ray launching method for wireless propagation prediction," in *IEEE 47th Vehicular Technology Conference. Technology in Motion*, 1997.
- [20] A. S. Glassner, *An Introduction to Ray Tracing - Real-Time Rendering*, San Diego: Elsevier, 1989.
- [21] Z. Zhang, Z. Yun and M. F. Iskander, "Ray tracing method for propagation models in wireless communication systems," *Electronics Letters*, vol. 36, no. 5, pp. 464-465, 2000.
- [22] R. Xu, "Light scattering: A review of particle characterization applications," *Particuology*, vol. 18, pp. 11-21, 2015.
- [23] S. Trajmar, D. F. Register and A. Chutjian, "Electron scattering by molecules II. Experimental methods and data," *Physics Reports*, vol. 97, no. 5, pp. 219-356, 1983.
- [24] F. Azevedo, A. Dias, J. Almeida, A. Oliveira, A. Ferreira, T. Santos, Alfredo Martins and E. Silva, "Lidar-based real-time detection and modeling of power lines for unmanned aerial vehicles," *Sensors*, vol. 19, no. 8, p. 1812, 2019.
- [25] R. González, J. Pearce and T. Lokki, "Modular design for spherical microphone arrays," in *Audio*

Engineering Society (AES) International Conference on Audio for Virtual and Augmented Reality, 2018.

- [26] A. J. Fenn, D. H. Temme, W. P. Delaney and W. E. Courtney, "The development of phased-array radar technology," *Lincoln Laboratory Journal*, vol. 12, no. 2, pp. 321-340, 2000.
- [27] S. S. Ahmed, A. Schiessl, F. Gumbmann, M. Tiebout, S. Methfessel and L.-P. Schmidt, "Advanced microwave imaging," *IEEE microwave magazine*, vol. 13, no. 6, pp. 26-43, 2012.
- [28] Y. Aron, "Turret indirect vision systems (TIVS) replacing episcopes on armored fighting vehicles," *Infrared Technology and Applications XLIII*, vol. 10177, p. 101770L, 2017.
- [29] V. Marsic, E. Kampert and M. D. Higgins, "Position Discrimination of a 2.4 GHz IEEE 802.15.4 RF Mobile Source Inside-Outside a Vehicle"," in *Proceedings of International Conference on Smart Applications, Communications and Networking (SmartNets 2021)*, 2021.